Mechanisms by which adiponectin reverses high fat diet-induced insulin resistance in mice

Xiruo Li[a,b], Dongyan Zhang[a], Daniel F. Vatner[a], Leigh Goedeke[a], Sandro M. Hirabara[a,c], Ye Zhang[a,d], Rachel J. Perry[a,b], and Gerald I. Shulman[a,b,1]

[a]Department of Internal Medicine, Yale School of Medicine, New Haven, CT 06520; [b]Department of Cellular and Molecular Physiology, Yale School of Medicine, New Haven, CT 06520; [c]Institute of Physical Activity Sciences and Sports, Cruzeiro do Sul University, 03342 Sao Paulo, Brazil; and [d]Department of Endocrinology & Metabolism, First Hospital of Jilin University, 130021 Changchun, Jilin, China

Adiponectin has emerged as a potential therapy for type 2 diabetes mellitus, but the molecular mechanism by which adiponectin reverses insulin resistance remains unclear. Two weeks of globular adiponectin (gAcrp30) treatment reduced fasting plasma glucose, triglyceride (TAG), and insulin concentrations and reversed whole-body insulin resistance, which could be attributed to both improved insulin-mediated suppression of endogenous glucose production and increased insulin-stimulated glucose uptake in muscle and adipose tissues. These improvements in liver and muscle sensitivity were associated with ~50% reductions in liver and muscle TAG and plasma membrane (PM)-associated diacylglycerol (DAG) content and occurred independent of reductions in total ceramide content. Reductions of PM DAG content in liver and skeletal muscle were associated with reduced PKCε translocation in liver and reduced PKCθ and PKCε translocation in skeletal muscle resulting in increased insulin-stimulated insulin receptor tyrosine1162 phosphorylation, IRS-1/IRS-2–associated PI3-kinase activity, and Akt-serine phosphorylation. Both gAcrp30 and full-length adiponectin (Acrp30) treatment increased eNOS/AMPK activation in muscle and muscle fatty acid oxidation. gAcrp30 and Acrp30 infusions also increased TAG uptake in epididymal white adipose tissue (eWAT), which could be attributed to increased lipoprotein lipase (LPL) activity. These data suggest that adiponectin and adiponectin-related molecules reverse lipid-induced liver and muscle insulin resistance by reducing ectopic lipid storage in these organs, resulting in decreased plasma membrane sn-1,2-DAG–induced nPKC activity and increased insulin signaling. Adiponectin mediates these effects by both promoting the storage of TAG in eWAT likely through stimulation of LPL as well as by stimulation of AMPK in muscle resulting in increased muscle fat oxidation.

adiponectin | lipoprotein lipase | ceramides | diacylglycerol | protein kinase C

Type 2 diabetes mellitus (T2DM) is one of the leading causes of morbidity and mortality in the adult population worldwide (1, 2) and is associated with disease in many organ systems, including nonalcoholic fatty liver disease (NAFLD) and atherosclerotic vascular disease (ASCVD) (3–6). Insulin resistance plays a critical role in the pathogenesis of T2DM and the metabolic syndrome. The adipokine adiponectin has emerged as a potential antidiabetic, antiinflammatory, and antiatherogenic factor (7, 8). Unlike adipokines such as leptin, plasma adiponectin levels are inversely correlated with adiposity and decreased in obesity, insulin resistance, and T2DM (9, 10). Adiponectin is present in human plasma as full-length adiponectin (Acrp30) and as a C-terminal globular fragment (gAcrp30) (11–13). The C-terminal globular fragment is produced by proteolytic cleavage and is thought to be the pharmacologically active moiety (11). A wide variety of explanations for adiponectin's glucose lowering and insulin sensitizing properties has been proposed, which have been derived predominantly from in vitro and ex vivo studies, including: suppression of gluconeogenesis (14–16), increased

AMPK/ACC-dependent fatty acid oxidation in liver and muscle (7, 12, 14, 17), and reduced hepatic ceramide content by activation of hepatic ceramidase (18). A clear, consistent model for adiponectin's action in vivo is lacking, and the mechanisms by which adiponectin ameliorates insulin resistance are a matter of active debate.

The association between ectopic lipid and insulin resistance in liver and skeletal muscle is widely recognized (19–21). Diacylglycerols (DAGs) and ceramides are the two best-studied mediators of lipid-induced insulin resistance. Ceramides have been shown to impair insulin action at the level of protein kinase B (Akt) phosphorylation, through activation of protein kinase Cζ (PKCζ) and/or protein phosphatase 2A (22–24). In contrast, plasma membrane sn-1,2-DAGs, which has been shown to be the key DAG stereoisomer, impair insulin action via activation of novel PKCs (nPKCs), including PKCε in liver (25–27) and both PKCθ and PKCε in skeletal muscle (28, 29). PKCε activation subsequently impairs insulin receptor kinase (IRK) tyrosine kinase activity, and PKCθ activation impairs insulin signaling at the level of IRS-1/IRS-2–associated PI3-kinase activity (20, 30, 31). Insulin resistance in the liver leads to reduced insulin-stimulated hepatic glycogen synthesis and defects in insulin suppression of hepatic glucose production, while insulin resistance in the skeletal muscle leads to reduced insulin-stimulated muscle glucose transport. In the setting of white adipose tissue (WAT) insulin

---

Significance

As it is estimated that one in three Americans will suffer from type 2 diabetes by 2050, interventions to ameliorate insulin resistance are of great interest. Adiponectin has emerged as a promising insulin-sensitizing adipokine; however, the mechanisms by which adiponectin administration improves insulin sensitivity are unclear. Here, we show that globular adiponectin (gAcrp30) and full-length adiponectin (Acrp30) reverse insulin resistance in HFD-fed mice through reductions in ectopic lipid in liver and muscle likely by stimulation of LPL activity in eWAT and increased eNOS/AMPK activation and fat oxidation in muscle. These effects, in turn, lead to decreased plasma membrane diacylglycerol content, resulting in decreased PKCε activation in liver and decreased PKCε/PKCθ activity in muscle and improved insulin signaling in these tissues.

---

resistance, WAT lipolysis is resistant to suppression by insulin, leading to increased nonesterified fatty acid (NEFA) delivery to the liver and muscle, which may further promote increased liver and muscle ectopic lipid content (4, 5, 32, 33).

Given that prior studies have demonstrated that increased plasma adiponectin concentrations lead to accretion of WAT and improved glycemia in mice (34, 35), we hypothesized that the insulin-sensitizing properties of adiponectin might be due to protection against ectopic lipid deposition in insulin-responsive tissues. To address this hypothesis, we performed a comprehensive series of studies to assess the effects of 2-wk gAcrp30 and Acrp30 treatment on multiple metabolic fluxes using a combination of stable- and radio-labeled isotopic tracers, in a high fat diet (HFD)-fed mouse model of lipid-induced insulin resistance. Here, we demonstrate that 2 wk of gAcrp30 treatment reverses whole-body insulin resistance in HFD-fed mice by reducing plasma membrane DAG content, resulting in decreased translocation of PKCε to the plasma membrane in liver and decreased PKCε/PKCθ translocation in skeletal muscle, leading to increased insulin signaling in both of these tissues. This reduction in ectopic lipid storage in liver and muscle could be attributed to increased lipoprotein lipase activity in epididymal WAT (eWAT), resulting in increased lipid uptake in eWAT, as well as activation of AMPK in muscle, which, in turn, promoted increased fatty acid oxidation in skeletal muscle. Taken together these results provide insights into the mechanisms by which adiponectin reverses insulin resistance in vivo.
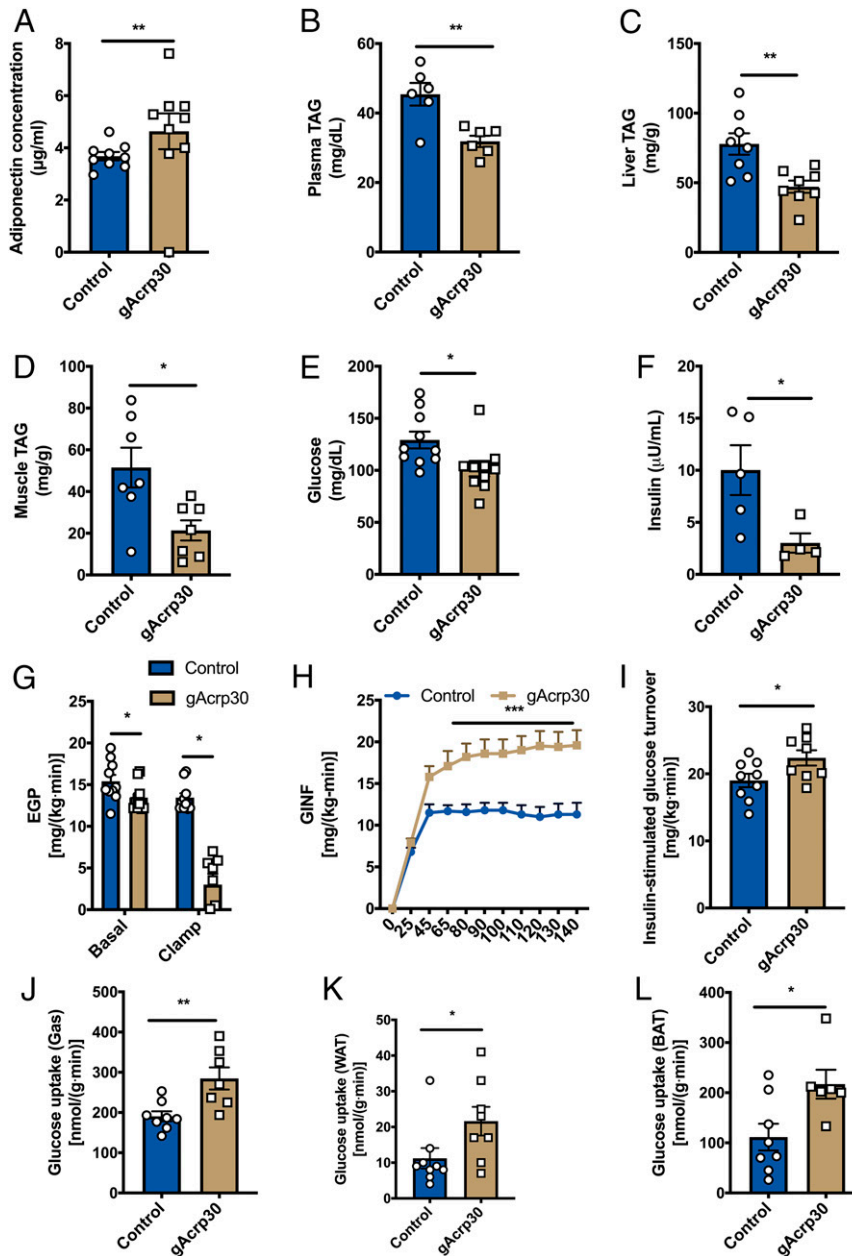
Results

Two-Week Globular Adiponectin Treatment Ameliorates Lipid-Induced Insulin Resistance.
In order to examine the effect of long-term exposure to increased globular adiponectin (gAcrp30) on glucose metabolism, we performed continuous subcutaneous (s.c.) gAcrp30 infusions (2.5 μg/d) in 12-wk HFD-fed mice for 2 wk. As expected, plasma adiponectin concentrations increased in the gAcrp30-treated mice compared with control mice (Fig. 1A). To assess the effect of gAcrp30 on energy balance, metabolic cages were utilized and whole-body energy expenditure was determined by indirect calorimetry. Consistent with the lack of difference in body weight or body composition (*SI Appendix*, Fig. S1 *A* and *B*), we observed no effect of gAcrp30 on whole-body oxygen consumption, carbon dioxide production, energy expenditure, caloric intake, respiratory exchange ratio, drinking, or activity (*SI Appendix*, Fig. S1 *C–I*).

While gAcrp30 did not alter whole-body energy metabolism, plasma triglyceride (TAG) concentrations as well as liver TAG content and muscle TAG content were significantly reduced by 35%, 45%, and 60%, respectively (Fig. 1 *B–D*). Consistent with a reduction in ectopic lipid content in liver and skeletal muscle, mice treated for 2 wk with gAcrp30 exhibited a 10% reduction in plasma glucose concentrations and a 65% reduction in plasma insulin concentrations after overnight fasting (Fig. 1 *E* and *F*). In contrast, there was no difference in fasting plasma NEFA concentration between groups (*SI Appendix*, Fig. S2A). In order to determine the effects of gAcrp30 on tissue-specific insulin action, we performed hyperinsulinemic-euglycemic clamps combined with radiolabeled and stable isotopes. Basal endogenous glucose production (EGP) was reduced by 13% in the gAcrp30 group as compared with the control group (Fig. 1G), resulting in reduced fasting plasma glucose concentrations (Fig. 1E). During the hyperinsulinemic phase of the clamp study, gAcrp30-treated mice displayed a twofold increase in the glucose infusion rate required to maintain euglycemia, reflecting increased whole-body insulin sensitivity (Fig. 1H and *SI Appendix*, Fig. S2 *B* and *C*). The increased whole-body insulin sensitivity could be attributed to both a twofold increase in insulin-mediated suppression of hepatic glucose production and a 15% increase in insulin-stimulated peripheral glucose disposal (Fig. 1 *G* and *I* and *SI Appendix*, Fig. S2D). Specifically, our data demonstrated that glucose uptake is increased by 50–100% in all assessed tissues, including skeletal muscle, WAT, and brown adipose tissue (Fig. 1 *J–L*).

Globular Adiponectin Reduces Plasma Membrane DAG Content and nPKC Activation in Liver and Skeletal Muscle.
As 2 wk of gAcrp30 treatment resulted in a marked improvement in liver and muscle insulin sensitivity, we next assessed insulin signaling pathways in the liver and skeletal muscle of these mice. Consistent with increased whole-body insulin sensitivity, gAcrp30-treated mice manifested twofold to fourfold increases in insulin-mediated insulin receptor tyrosine autophosphorylation (tyrosine 1162) in both liver and skeletal muscle (Fig. 2 *A* and *B*). We also observed fourfold increases in insulin-stimulated insulin receptor substrate-2 (IRS-2)–associated phosphoinositide 3-kinase (PI3K) activity in liver and IRS-1–associated PI3K activity in muscle, as well as twofold increases in Akt2 phosphorylation in liver and skeletal muscle of gAcrp30-treated mice as compared with vehicle-treated mice in the clamp state (Fig. 2 *C–F*), indicating improved insulin signaling in liver and muscle. Activated c-Jun N-terminal kinase (JNK) can phosphorylate insulin receptor substrate-1 (IRS-1) serine 302, resulting in negative regulation of the insulin signaling pathway in mouse tissues (7, 36). This mechanism may play a role in the improved insulin sensitivity seen in gAcrp30-treated mice, as we observed an ~40% decrease in JNK phosphorylation in liver and muscle from animals treated with gAcrp30 vs. vehicle-treated animals (*SI Appendix*, Fig. S2 *E* and *F*), which may in part be due to adiponectin's effect on reducing oxidative stress (7).

DAGs and ceramides are two well-studied bioactive lipids that have been proposed to mediate lipid-induced insulin resistance (27). Plasma membrane DAGs have been shown to mediate insulin resistance by activation of nPKCs, specifically PKCε in the liver and both PKCε and PKCθ in the skeletal muscle (25, 30, 37, 38). Among the three stereoisomers of DAG (sn-1,2-DAG, sn-1,3-DAG, and sn-2,3-DAG), sn-1,2-DAG is thought to be primarily responsible for nPKC activation (39–41). To understand the mechanism by which gAcrp30 treatment ameliorates lipid-induced liver and muscle insulin resistance, DAG content, ceramide content, and nPKC translocation were measured in these tissues. Hepatic plasma membrane sn-1,2-DAG was decreased by 35% in gAcrp30-treated mice, which was associated with a ~50% reduction in PKCε membrane translocation, reflecting reduced PKCε activation (Fig. 2 *G* and *H*). Plasma membrane sn-2,3-DAG content was decreased by 35% without any difference in sn-1,3-DAG content and sn-1,2-DAG content in other subcellular compartments (*SI Appendix*, Fig. S2 *G–I*). INSR Thr1160 is a PKCε target, upon which phosphorylation impairs the tyrosine kinase activity of the insulin receptor and, thereby, diminishes downstream insulin signaling (25, 40). Consistent with reductions in PKCε activity and improved hepatic insulin sensitivity, hepatic insulin receptor Thr1160 phosphorylation was decreased in gAcrp30-treated mice (Fig. 2I). Similarly, in the gastrocnemius muscle, gAcrp30-treated mice exhibited an ~55% reduction in plasma membrane DAG content with an associated 60–80% reduction in PKCθ and PKCε translocation (Fig. 2 *J–L*). In contrast, despite the reductions in liver and muscle TAG content, plasma membrane DAG content, and marked reversal of insulin resistance in liver and skeletal muscle, there were no significant changes in total ceramide content in these tissues (Fig. 2 *M* and *N*), arguing against an important role for adiponectin-induced activation of ceramidase as the insulin-sensitizing mechanism by which adiponectin would have been expected to lead to a reduction in total ceramide content (18). In addition, we did not observe any significant differences in the total content of specific ceramide species (C16:0 and C18:0), which have been specifically hypothesized to mediate insulin resistance in rodents (42, 43) (*SI Appendix*, Fig. S2 *J–M*). While gAcrp30 treatment did not cause a reduction in total tissue ceramide content, it did result in reductions in several hepatic ceramide species (C16:0, C20:0, C22:0, C24:0, and C24:1) in the

Fig. 1. Globular adiponectin treatment ameliorates lipid-induced insulin resistance in HFD-fed mice. (*A*) Plasma adiponectin concentrations after overnight fasting in HFD-fed mice treated with globular adiponectin (gAcrp30) or vehicle-control for 2 wk. (*B*) Plasma TAG concentrations of control and gAcrp30-treated mice after overnight fasting. (*C* and *D*) Liver and muscle TAG content of control and gAcrp30-treated mice. (*E* and *F*) Plasma glucose (*n* = 10) and insulin concentrations (*n* = 4–5) of control and gAcrp30-treated mice after overnight fasting. (*G*) Endogenous glucose production rate under basal and the hyperinsulinemia-euglycemia clamp states (*n* = 8–10). (*H*) Glucose infusion rate during the hyperinsulinemic-euglycemic clamp. (*I*) Glucose turnover rate during the hyperinsulinemia-euglycemia clamp. (*J–L*) Insulin-stimulated glucose uptake rate in skeletal muscle, WAT, and brown adipose tissue in control and gAcrp30-treated mice. Data are shown as mean ± SEM *P < 0.05 by two-way ANOVA with Dunnett multiple comparisons for *G*. *P < 0.05, **P < 0.01, ***P < 0.001 by unpaired Student's *t* test for other graphs.

plasma membrane (*SI Appendix*, Fig. S2*N*), which correlated with the improved insulin sensitivity in liver.
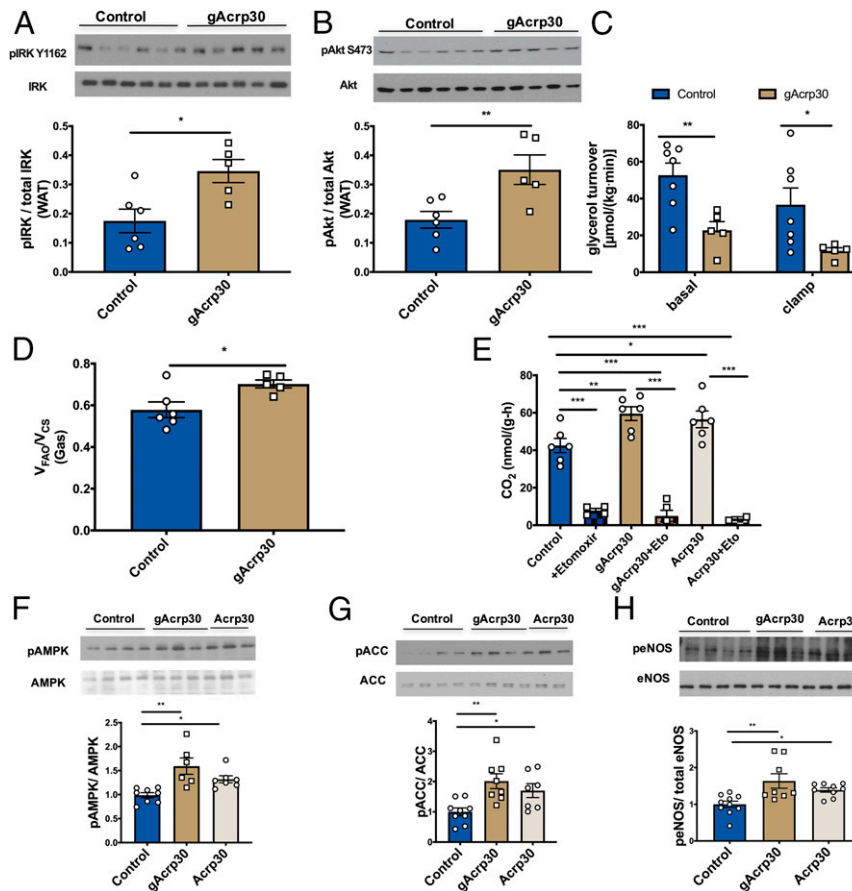
gAcrp30 Improves Insulin Signaling in WAT. Next, we sought to understand the effect of gAcrp30 treatment on insulin signaling in WAT and on WAT lipolysis. gAcrp30 administration increased phosphorylation of IRK and Akt2, and reduced phosphorylation of perilipin, adipose TAG lipase (ATGL), and hormone-sensitive lipase (HSL) in the clamp state, indicating improved insulin signaling in WAT (Fig. 3 *A* and *B* and *SI*

Appendix, Fig. S3 *A–C*). Consistent with these data, gAcrp30-treated mice had reduced whole-body glycerol turnover rate in the basal and clamp state, demonstrating that gAcrp30 treatment reduced WAT lipolysis and improved insulin signaling in WAT (Fig. 3*C*). Reduced glycerol conversion to glucose may result in reduced hepatic glucose production and plasma glucose concentrations (44). However, surprisingly, there were no differences in the whole-body fatty acid turnover rate or plasma NEFA concentrations (*SI Appendix*, Fig. S3 *D* and *E*), suggesting that gAcrp30 may also promote WAT reesterification. Consistent with
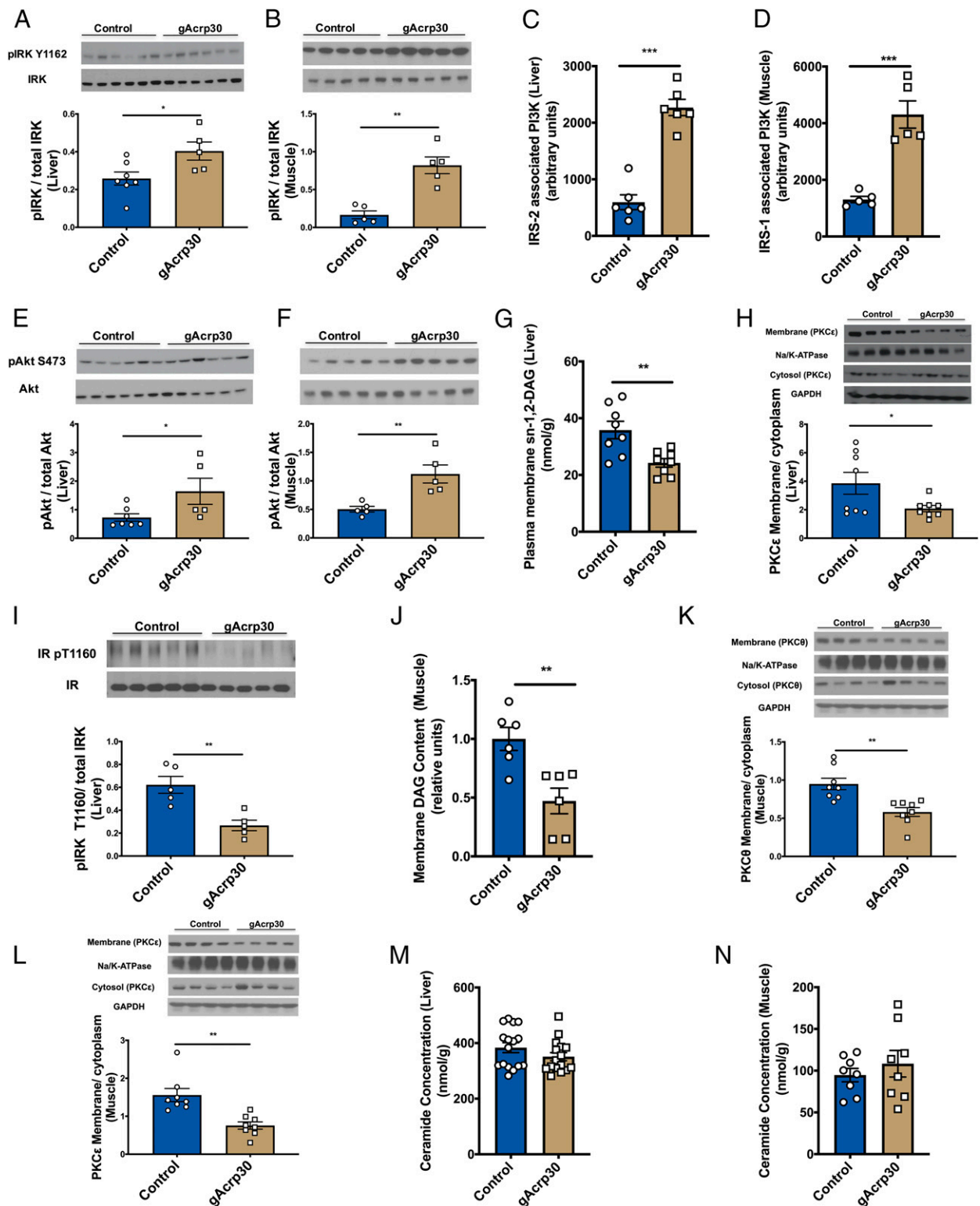
Fig. 2. Globular adiponectin reduces membrane DAG content and nPKC activation in liver and muscle. (*A* and *B*) Western blot images for insulin receptor kinase phosphorylation (pY1162) in liver (*n* = 5–7) and skeletal muscle (*n* = 5) of control and gAcrp30-treated mice under the hyperinsulinemic-euglycemic clamp condition. Quantification is shown below. (*C*) IRS–2–associated PI3K activity in liver. (*D*) IRS–1–associated PI3K activity in muscle (*n* = 5). (*E* and *F*) Western blot images for Akt phosphorylation (pS473) in liver (*n* = 5–7) and skeletal muscle (*n* = 5) in the clamp state. Quantification is shown below. (*G*) Hepatic plasma membrane *sn*-1,2-DAG content. (*H*) Hepatic membrane/cytosolic PKCε ratio. Quantification is shown below. (*I*) Western blot images for insulin receptor kinase phosphorylation (pY1160) in liver (*n* = 5). Quantification is shown below. (*J*) Membrane DAG content in skeletal muscle. (*K* and *L*) Membrane/cytosolic PKCθ and PKCε ratio in skeletal muscle. PKCθ and PKCε were probed from the same membrane and therefore have the same corresponding loading controls (GAPDH and Na/K-ATPase). Quantification is shown below. (*M* and *N*) Total ceramide content in liver (*n* = 16) and skeletal muscle. Data are shown as mean ± SEM *P < 0.05, **P < 0.01, ***P < 0.001 by unpaired Student's t test.

MEDICAL SCIENCES

Fig. 3. gAcrp30 improves insulin signaling in WAT and increases the switch from glucose to fat oxidation in skeletal muscle in vivo. (*A*) Western blot images for insulin receptor kinase phosphorylation (pY1162) in WAT (*n* = 5–6) in the clamp state. Quantification is shown below. (*B*) Western blot images for Akt phosphorylation (pS473) in WAT (*n* = 5–6) in the clamp state. Quantification is shown below. (*C*) Glycerol turnover rate under basal and hyperinsulinemic-euglycemic conditions (*n* = 5–7). (*D*) Ratio of mitochondrial ketone oxidation and β-oxidation (V_{FAO}) to citrate synthase flux (V_{CS}) in soleus muscle (*n* = 5–6). (*E*) Fatty acid oxidation rates of solus muscles with no treatment (control), control + etomoxir, gAcrp30 treatment, gAcrp30 + etomoxir, Acrp30 treatment, Acrp30 + etomoxir (*n* = 2–6). (*F–H*) Representative Western blot images for nontreated, gAcrp30-treated, and Acrp30-treated AMPK, ACC, and endothelial nitric-oxide synthase phosphorylation in soleus muscle. Quantification is shown below. Data are shown as mean ± SEM *$P < 0.05$, **$P < 0.01$ by two-way ANOVA with Dunnett multiple comparisons for *C*. *$P < 0.05$, **$P < 0.01$, ***$P < 0.001$ by one-way ANOVA with Tukey multiple comparisons for *E–H*. *$P < 0.05$, **$P < 0.01$ by unpaired Student's *t* test for other graphs.

the lack of differences in fatty acid turnover, we observed no differences in hepatic acetyl-CoA, malonyl-CoA, or long-chain acyl-CoA concentrations (*SI Appendix*, Fig. S3 *F–H*). Taken together, these data indicate that gAcrp30 treatment also improves insulin signaling in WAT and may affect WAT lipolysis and reesterification.

Globular Adiponectin Treatment Promotes a Switch from Glucose to Fat Oxidation in Skeletal Muscle. In order to determine whether the reduction in ectopic lipid (TAG/DAG) content could be attributed to increased fatty acid oxidation in liver and muscle, we assessed mitochondrial function in vivo and ex vivo. We employed positional isotopomer NMR tracer analysis (PINTA) to assess the effects of gArcp30 on in vivo hepatic citrate synthase flux (V_{CS}, i.e., mitochondrial oxidation) and hepatic pyruvate carboxylase flux (V_{PC}, i.e., gluconeogenesis from pyruvate) (45) and observed no significant differences in hepatic V_{PC} or V_{CS} in gAcrp30-treated mice (*SI Appendix*, Fig. S3 *I* and *J*). In addition, there was no difference in the phosphorylation of two key regulators of hepatic fatty acid oxidation and biosynthesis: 5′ AMP-activated protein kinase (AMPK) and acetyl-CoA carboxylase (ACC) with gAcrp30 treatment (*SI Appendix*, Fig. S3 *K* and *L*). In summary, no differences were observed in

hepatic mitochondrial oxidation rate or its upstream regulators or downstream outflow (V_{PC}) in the gAcrp30-treated mice.

Relative rates of mitochondrial ketone oxidation and β-oxidation (V_{FAO}) normalized to citrate synthase flux (V_{CS}) were determined in vivo in multiple tissues. gAcrp30 treatment promoted a shift away from glucose to other substrates (fatty acids, ketones, ketogenic amino acids) in gastrocnemius muscle (Fig. 3*D*), despite no effect on liver or quadriceps muscles (*SI Appendix*, Fig. S3 *M* and *N*). To further examine the effects of gAcrp30 on absolute rates of fatty acid oxidation and glucose oxidation in muscle, we assessed rates of $^{14}CO_2$ production in isolated soleus muscle with [1-^{14}C]palmitic acid and [$^{14}C_6$]D-glucose as substrates. Consistent with the in vivo gastrocnemius data, both fatty acid oxidation and glucose oxidation were increased in the Acrp30-treated and gAcrp30-treated soleus muscles (Fig. 3*E* and *SI Appendix*, Fig. S3*O*). To understand the potential molecular mechanisms by which fatty acid oxidation was increased in the soleus muscle, we measured phosphorylation of AMPK, ACC, and endothelial nitric oxide synthase (eNOS). Previous studies have shown that there is a positive feedback loop between nitric oxide production and AMPK activation (46). Consistent with these studies, we observed significant increases in phosphorylation of AMPK, ACC, and eNOS in the skeletal muscle of both Acrp30-treated and gAcrp30-treated mice (Fig. 3 *F–H*).

These data suggest that gAcrp30 and Acrp30 treatment activates the eNOS/AMPK/ACC pathway and promotes a switch from glucose oxidation to fatty acid oxidation in predominately slow-twitch gastrocnemius and soleus muscles but does not impact hepatic mitochondrial fat oxidation.

Globular Adiponectin and Full-Length Adiponectin Increase Lipoprotein Lipase Activity and Lipid Uptake in eWAT. To determine whether adiponectin treatment alters ectopic lipid deposition by changing TAG-rich lipoprotein metabolism, we performed a series of studies assessing very-low-density lipoprotein (VLDL) production and chylomicron clearance. We first measured the rates of hepatic VLDL-TAG production to evaluate whether hepatic VLDL-TAG production contributed to the reduced plasma TAG in the gAcrp30-treated mice. No significant difference in the hepatic VLDL-TAG production rate with gAcrp30 treatment was observed (*SI Appendix*, Fig. S4 *A and B*). Then, we tested the hypothesis that the reductions in TAGs and membrane DAGs in liver and skeletal muscle may be explained by increased uptake of lipids into WAT, thereby diverting circulating TAGs away from

storage in liver and skeletal muscle. Consistent with the hypothesis, plasma lipid clearance was increased during an oral lipid tolerance test in the gAcrp30-treated mice (Fig. 4 *A and B*). gAcrp30 treatment promoted increased lipid uptake in eWAT despite no significant difference in lipid uptake in s.c. WAT (sWAT) or skeletal muscle (Fig. 4 *C and D* and *SI Appendix*, Fig. S4C).

Lipoprotein lipase (LPL) plays an important role in the clearance of plasma TAG and the import of TAG-derived fatty acid to muscle and heart for utilization and adipose tissues for storage (47). We measured plasma and tissue-specific LPL activity to assess whether gAcrp30 alters adipose chylomicron clearance via alterations in LPL activity. gAcrp30-treated mice have increased heparin-releasable LPL activity in plasma and increased LPL activity in eWAT and heart (Fig. 4 *E–G*). In contrast, there were no significant effects of gAcrp30 treatment on sWAT, brown adipose tissue (BAT), or skeletal muscle LPL activity (Fig. 4*H* and *SI Appendix*, Fig. S4 *D and E*).

It has previously been shown that Acrp30 also reduces plasma and tissue TAG content in mice liver and skeletal muscle (48,
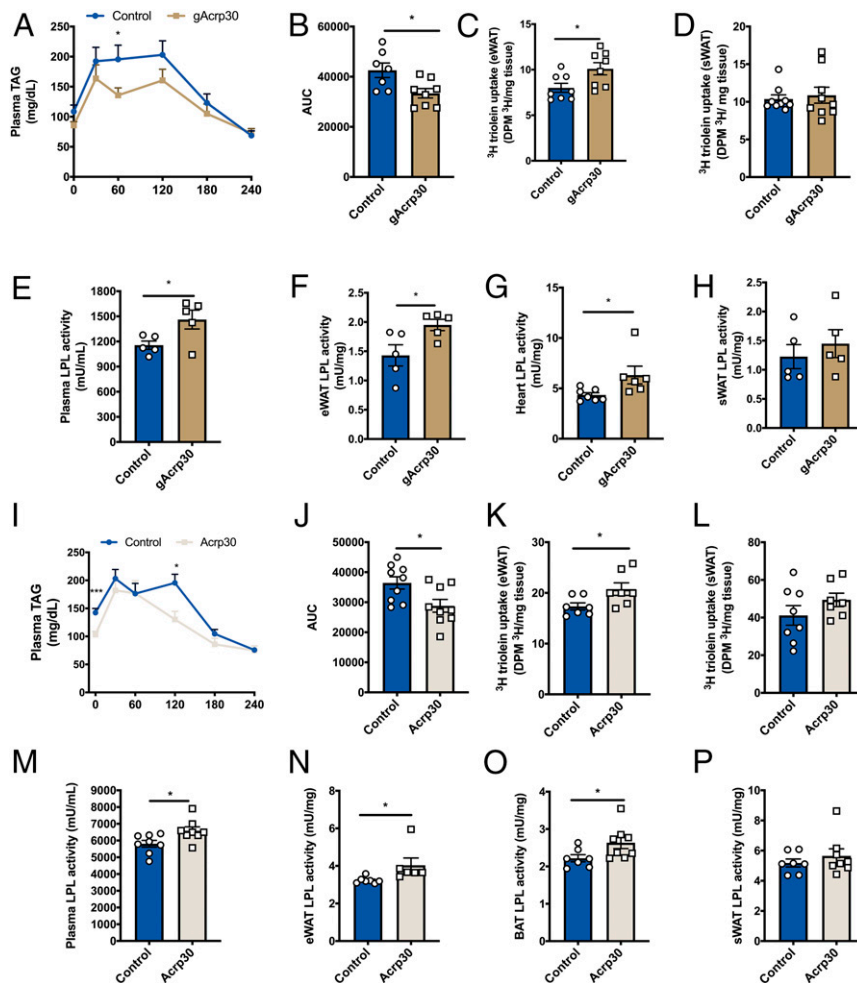
Fig. 4. Globular adiponectin and full-length adiponectin increase lipoprotein lipase activity and lipid uptake in epididimal WAT. (*A*) Plasma TAG concentrations of control and gAcrp30-treated mice during oral lipid tolerance test. (*B*) Area under the plasma TAGs curve of control and gAcrp30-treated mice. (*C and D*) TAG uptake in epididimal WAT (*n* = 8–10) and s.c. WAT of control and gAcrp30-treated mice. (*E*) Postheparin plasma LPL activity of control and gAcrp30-treated mice (*n* = 5). (*F*) eWAT LPL activity of control and gAcrp30-treated mice (*n* = 5). (*G*) Heart LPL activity of control and gAcrp30-treated mice. (*H*) s.c. white adipose LPL activity of control and gAcrp30-treated mice (*n* = 5). (*I*) Plasma TAG concentrations of control and Acrp30-treated mice during oral lipid tolerance test. (*J*) Area under the plasma TAGs curve of control and Acrp30-treated mice. (*K and L*) TAG uptake in eWAT and sWAT of control and Acrp30-treated mice. (*M*) Postheparin plasma LPL activity of control and Acrp30-treated mice. (*N*) eWAT LPL activity of control and Acrp30-treated mice. (*O*) Brown adipose tissue LPL activity of control and Acrp30-treated mice. (*P*) s.c. white adipose LPL activity of control and Acrp30-treated mice. Data are shown as mean ± SEM *$P < 0.05$, ***$P < 0.001$ by unpaired Student's *t* test.

49). To determine whether the decreased TAG content by Acrp30 could be explained by similar mechanisms as gAcrp30 treatment, we performed continuous s.c. Acrp30 infusions (10 µg/d) in HFD-fed mice for 2 wk and a series of studies assessing chylomicron clearance and LPL activity. As expected, plasma TAG was decreased with Acrp30 treatment (Fig. 4*I*). Analogous to what we observed in gAcrp30 treated mice, 2-wk Acrp30 treatment increased lipid clearance during the oral lipid tolerance test and improved lipid uptake in eWAT, without significant difference in lipid uptake in sWAT or skeletal muscle (Fig. 4 *I–L* and *SI Appendix*, Fig. S4*F*). Acrp30 infusion also increased heparin-releasable plasma LPL activity and increased LPL activity in eWAT and BAT (Fig. 4 *M–O*). No significant differences in sWAT, heart, and muscle were observed (Fig. 4*P* and *SI Appendix*, Fig. S4 *G* and *H*). Taken together, these data demonstrate that both full-length and globular adiponectin treatment enhances lipid uptake in eWAT, which may be attributed to localized stimulation of LPL activity in eWAT.

Discussion

WAT is not only a critical energy storage depot, but it also acts as an endocrine organ sensing metabolic signals and secreting hormones and adipocytokines (e.g., leptin and adiponectin) that regulate whole-body energy homeostasis (50–53). Consistent with previous reports (14, 15, 17), we have demonstrated that administration of globular adiponectin results in an improvement in whole-body glucose homeostasis. Despite great interest in adiponectin, the mechanism by which adiponectin reverses insulin resistance remains unclear. To address this question, we performed a comprehensive series of studies including hyperinsulinemic-euglycemic clamp studies combined with stable-labeled and radio-labeled isotopic tracers to characterize adiponectin's effects on endogenous glucose production and tissue-specific insulin sensitivity and followed these studies up by measuring bioactive lipid metabolites and cellular insulin signaling phosphorylation events in liver, skeletal muscle, and WAT.

Adiponectin receptor associated ceramidase activity, promoting decreased total hepatic ceramide content and ceramide-induced insulin resistance, has been proposed to mediate adiponectin's insulin-sensitizing properties (18). However, in contrast to this hypothesis, we dissociated changes in total ceramide content in the liver and skeletal muscle from gAcrp30-induced improvements in liver and muscle insulin sensitivity. We also did not observe any significant differences in the content of specific ceramide species (C16:0 and C18:0), which have been specifically hypothesized to mediate insulin resistance in rodents (42, 43). While gAcrp30 treatment did not cause a reduction in total tissue ceramide content or in changes in C16:0 or C18:0 ceramides, it did result in reductions in several hepatic ceramide species (C16:0, C20:0, C22:0, C24:0, and C24:1) in the plasma membrane, which correlated with improved insulin sensitivity in liver. Whether these specific plasma membrane-associated ceramide species also contributed to alterations in insulin action will need to be examined in future studies.

Nevertheless, ceramide-induced insulin resistance is thought to alter downstream insulin signaling at the level of Akt; however, we observed that gAcrp30 improved insulin action at the level of the insulin receptor, which is not compatible with the putative mechanisms by which adiponectin is thought to mediate insulin resistance at the level of AKT2 phosphorylation.

In contrast with ceramide-induced insulin resistance, DAG-PKCε–induced insulin resistance can explain improved insulin signaling at the level of the insulin receptor. By this mechanism, *sn*-1,2-DAG accumulation in the plasma membrane of liver and muscle results in nPKC translocation from the cytoplasm to the plasma membrane, leading to decreased insulin signaling at the level of the insulin receptor due to PKCε activation and at the level of IRS-1–associated and IRS-2–associated PI3-kinase due

to PKCθ activation (25, 26, 30). We observed that 2 wk of gAcrp30 treatment reduced plasma membrane *sn*-1,2-DAG in liver and membrane-associated DAG in muscle, leading to decreased PKCε activity in liver and both PKCθ and PKCε activity in skeletal muscle. As a result, insulin signaling at the level of insulin receptor kinase increased in both of these tissues. As such, the effect of globular adiponectin on tissue-specific insulin action appears to occur through reductions in liver and muscle plasma membrane DAG content, resulting in reduced PKCε activation in liver and reduction in both PKCε and PKCθ activation in skeletal muscle.

In both in vitro and ex vivo studies, adiponectin has been suggested to reduce TAG content in the liver and muscle by enhancing fatty acid oxidation in an AMPK-dependent manner (7, 12, 14, 54, 55). However, Yamauchi et al. found that globular adiponectin cannot activate hepatic AMPK signaling pathways (48). No competing hypothesis has yet been published, and so the underlying physiological mechanisms by which gAcrp30 reduces hepatic TAG are still debated. Further complicating this question, most mechanistic studies examining adiponectin's mechanism of action have been performed purely in vitro and ex vivo, whereas in vivo studies are critical to understand the complex interorgan cross-talk that regulates metabolic physiology. Reduced ectopic lipid content in liver and skeletal muscle may be due to several factors including 1) decreased NEFA flux to these tissues from reduced WAT lipolysis; 2) increased rates of tissue mitochondrial fatty acid oxidation; and 3) decreased lipid delivered to tissues from circulating lipoproteins. We evaluated each of these potential mechanisms for the gAcrp30-induced reductions in ectopic lipids in HFD-fed mice using a comprehensive series of in vivo metabolic studies. While gAcrp30 appeared to suppress rates of WAT lipolysis, as reflected by reduced rates of glycerol turnover and increased WAT insulin sensitivity, as reflected by increased insulin-stimulated glucose uptake, it did not affect whole-body fatty acid turnover potentially due to compensatory changes in reesterification. Additionally, hepatic mitochondrial fatty acid oxidation and the regulation of fat oxidation in liver were unchanged. In gastrocnemius and soleus muscle, gAcrp30 treatment increases muscle fatty oxidation in vivo and ex vivo, an effect that was correlated with increased phosphorylation of ACC in a manner consistent with previously described eNOS/AMPK-dependent regulation of ACC (46). This increase in skeletal muscle fatty acid oxidation could account, in part, for the reduced ectopic lipid deposition seen in several tissues in gAcrp30-treated mice and the improvement in muscle insulin sensitivity.

In addition to promoting increased muscle fatty acid oxidation, we also found that both gAcrp30 and Acrp30 treatment reduces ectopic lipid (TAG/plasma membrane DAG) accumulation in liver and skeletal muscle by improving WAT TAG uptake and further increasing WAT storage capacity. Adiponectin-treated mice displayed increased LPL activity in postheparin plasma and eWAT and improved adipose postprandial triacylglycerol uptake. These results are consistent with our observations that 2 wk of gAcrp30 or Acrpt30 treatment increased eWAT mass but did not change total fat mass, as assessed by ^{1}H NMR.

Our findings also imply an important role for decreased plasma adiponectin in the development of lipid-induced liver and skeletal muscle insulin resistance. In humans and monkeys, plasma adiponectin levels correlate significantly with whole-body insulin sensitivity (56, 57). Overexpression or administration of adiponectin in mice results in a decrease in hyperglycemia and improvement in systemic insulin sensitivity (7, 58), whereas adiponectin-deficient mice exhibit impaired insulin sensitivity and are prone to diabetes (8, 59). Tying all of this together, circulating adiponectin may be a reflection of the presence of functioning adipose tissue, a part of the machinery the WAT uses in its fat-storing operation. In normal physiology, healthy

adipose tissue secretes sufficient adiponectin to promote storage of circulating TAG in WAT and signal a shift to increase fatty acid oxidation in skeletal muscle. However, in obesity, as adipose tissue has limited storage capacity, WAT secretion of adiponectin decreases. This derangement in fat storage and muscle fat oxidation may then lead to increased ectopic lipid (TAGs/plasma membrane DAGs) accumulation in liver and skeletal muscle and the subsequent development of insulin resistance in these organs leading to the metabolic syndrome, hepatic steatosis/NASH, and atherosclerosis.

Taken together, these results suggest that chronic adiponectin administration ameliorates insulin resistance in an HFD-fed mouse model of obesity, NAFLD, and insulin resistance by two major mechanisms. First, adiponectin treatment promotes increased WAT LPL activity, which may lead to increased uptake of TAG into WAT, thus diverting circulating TAG away from storage in liver and skeletal muscle. Second, adiponectin treatment promotes increased fatty acid oxidation in skeletal muscle, which, in turn, may be attributed to the activation of AMPK and eNOS. These two effects of adiponectin, in turn, lead to reductions in liver and muscle plasma membrane-associated sn-1,2-DAG content, resulting in decreased PKCε activity in liver and decreased PKCε and PKCθ in muscle resulting in increased insulin signaling and insulin action in these tissues. Furthermore, adiponectin-induced improvement in liver and muscle insulin sensitivity in insulin-resistant, HFD-fed mice occurred independently of changes in total ceramide content in these tissues. Taken together, these studies provide insights into the mechanisms by which adiponectin reverses HFD-induced liver and muscle insulin resistance in mice.

Materials and Methods

Animals. All rodent studies were approved by the Yale University Institutional Animal Care and Use Committee. Male C57BL/6J mice (Jackson Laboratory) were group housed at the animal care facility at Yale University Animal Research Center and maintained under controlled temperature (23 °C) and lighting (12:12 h light/dark cycle, lights on at 7:00 A.M.) with free access to water and food. Diet-induced obesity studies were carried out by feeding mice a HFD (60% calories from fat, Research Diets D12492). To study the effects of adiponectin treatment, following 2 wk or 10 wk of HFD, mini-osmotic pumps (Alzet) containing recombinant mouse globular adiponectin protein (Abcam), recombinant mouse full-length adiponectin (Abcam), or vehicle (saline) were implanted s.c.. Adiponectin was released at a rate of 2.5 μg/d (globular adiponectin) or 10 μg/d (full-length adiponectin) for 14 d based on previous literature (14, 48). Food and water intake measurements and indirect calorimetry were performed using Columbus Lab Animal Monitoring System metabolic cages (Columbus Instruments). During this time, food intake and body weight were regularly monitored. The mice used for euglycemic clamp and in vivo tracer studies underwent surgery under isoflurane anesthesia to place catheters in the jugular vein and single-housed mice were allowed to recover 6–7 d before planned experiments.

Hyperinsulinemic-Euglycemic Clamps. Clamps were performed as previously described (26, 60). Briefly, after an overnight fast, a 120-min basal infusion with [3-³H] glucose (PerkinElmer) at a rate of 0.05 μCi/min, [1,1,2,3,3-D₅] glycerol (Sigma Aldrich) at a rate of 1.5 μmol/(kg·min) and potassium [¹³C₁₆] palmitate (Cambridge Isotopes) at a rate of 0.7 μmol/(kg·min) was performed. After the basal period, mice underwent a 140-min hyperinsulinemic-euglycemic clamp by infusing [3-³H] glucose, [1,1,2,3,3-D₅] glycerol, and potassium [¹³C₁₆] palmitate at the rates indicated above, and in the last 55 min of the clamp period, 2-deoxy-[1-¹⁴C] glucose (2-DG) (PerkinElmer) was given to estimate tissue-specific glucose uptake. Twenty percent dextrose (Hospira) at a variable rate and insulin at a rate of 3 mU/[kg·min] was infused through the jugular venous catheter to maintain a steady-state plasma glucose concentration of ~120 mg/dL. Plasma glucose concentrations were measured every 10–15 min during the hyperinsulinemic-euglycemic clamp period. At the end of the study, mice were euthanized with intravenous (i.v.) pentobarbital and tissues were obtained following the clamp study using freeze clamps precooled in liquid nitrogen. The specific activity of glucose was measured in plasma samples collected at the steady state during basal and clamp by liquid scintillation counting.

Flux Measurement. Positional isotopomer NMR tracer analysis (PINTA) was applied to measure rates of hepatic mitochondrial citrate synthase flux (V_{CS}) and pyruvate carboxylase flux (V_{PC}) as previously described (45). Infusion of [3-³H] glucose (PerkinElmer) at a rate of 0.05 μCi/min and [3-¹³C] sodium lactate (Cambridge Isotopes) at a rate of 40 μmol/(kg·min) was performed for a total of 120 min to measure V_{PC}/V_{CS} and V_{PC}/V_{EGP} as we previously described (45).

The ratio of pyruvate dehydrogenase flux to citrate synthase flux (V_{PDH}/V_{CS}) was used to indicate tissue-specific metabolic substrate oxidation after a 2-h infusion of [1,2,3,4,5,6-¹³C₆]glucose (16.7 μmol/[kg·min] prime for 5 min, 5.6 μmol/[kg·min] continuous infusion) as previously described (61). Briefly, V_{PDH}/V_{CS} was measured as the ratio of [4,5-¹³C₂]glutamate/[¹³C₃]alanine. [¹³C₃]alanine enrichment was measured by gas chromatography–mass spectrometry (GC/MS) and [4,5-¹³C₂]glutamate enrichment was measured by liquid chromatography–tandem mass spectrometry (LC-MS/MS) as previously described (29).

[1,1,2,3,3-D₅]glycerol and [¹³C₁₆]palmitate enrichments were measured using GC/MS as previously described (61). Briefly, glycerol turnover = ([1,1,2,3,3-D₅] glycerol tracer enrichment/[1,1,2,3,3-D₅] glycerol plasma enrichment − 1) x infusion rate. Palmitate turnover = ([¹³C₁₆] palmitate tracer enrichment/[¹³C₁₆] palmitate plasma enrichment − 1) x infusion rate. Fatty acid turnover = Palmitate turnover rate/(palmitate/total fatty acids).

Palmitate and Glucose Oxidation Measurement Ex Vivo. Ex vivo muscle oxidation measurements were performed as previously described (62) with minor modifications. Briefly, mice were fasted overnight (12 h) before the procedure. Animals were euthanized during tissue collection under isoflurane anesthesia; intact soleus muscles were rapidly removed and pinned in stainless steel clips to maintain resting tension. Muscles were pre-incubated in Krebs–Ringer bicarbonate buffer (KRBB), with 10 mM glucose and 0.5% BSA, pH 7.4, at 35 °C, for 30–45 min. Soleus muscles were then incubated in the same buffer containing either radiolabeled palmitic acid (0.1 mM palmitic acid [Sigma Aldrich] and 0.2 μCi/mL [1-¹⁴C]palmitic acid [PerkinElmer]) or radiolabeled glucose (10 mM glucose [Sigma Aldrich] and 0.2 μCi/mL [¹⁴C₆]ᴅ-glucose [PerkinElmer]) for 1 h. ¹⁴CO₂ produced was trapped in NaOH (0.3 mL at 2 N) during incubation. Muscles were removed, washed in cold saline for 1 min, blotted on filter paper, and weighed. Incubation vials were tightly capped, and 0.5 mL of 2 N HCl was added directly to the KRBB using a syringe; vials were incubated for 2 h at 37 °C. ¹⁴CO₂ absorbed in NaOH solution was then quantified by scintillation counting.

Biochemical Analysis. Plasma glucose was measured enzymatically using a YSI Glucose Analyzer (YSI). Plasma insulin concentrations were measured by RIA (EMD Millipore) at the Yale Diabetes Research Center. Plasma NEFA and TAG concentrations were measured by standard spectrophotometric assays (NEFA: Wako Diagnostics; TAG: Sekisui/Fujifilm). Plasma adiponectin (full-length and globular adiponectin) concentrations were measured by enzyme-linked immunoassay (ELISA) (Abcam).

Tissue Analysis. Liver DAG stereoisomers in five subcellular compartments were measured as previously described (40, 63). Briefly, liver tissues were first homogenized with a Doucne-type homogenizer in cold (4 °C) TES buffer (250 mM sucrose, 10 mM Tris at pH 7.4, 0.5 mM EDTA). Then, the homogenate was centrifuged (at 12,000 rpm with SS-34 rotor or 17,000 × g, 15 min, 4 °C) to obtain pellet A and supernatant A. The top lipid layer was collected as the lipid droplet fraction. The supernatant A was washed, centrifuged, and then resuspended in TES buffer and gently layered on top of 1.12 M sucrose buffer cushion in ultracentrifuge tubes. Then it was centrifuged (at 35,000 rpm with TLS-55 rotor or 105,000 × g, 20 min, 4 °C) to obtain pellet B, interface B, and supernatant B. The interface B was collected, washed, and centrifuged to get plasma membrane fraction. The pellet B was washed and centrifuged to obtain mitochondria fraction. The supernatant B was centrifuged (at 65,000 rpm with Ti-70.1 rotor or 390,000 × g, 75 min, 4 °C) to separate pellet C and supernatant C. Pellet C was washed, centrifuged, and collected as the endoplasmic reticulum fraction. Supernatant C was collected as the cytosol fraction. DAG and ceramide concentrations (30), hepatic long-chain acyl-CoA (30), acetyl-CoA, and malonyl-CoA (60) were measured as previously described.

Tissue TAG content was measured by a standard kit (Sekisui/Fujifilm) after extraction by the method of Bligh and Dyer (64). For nPKC translocation, cytoplasm and plasma membrane fractions were separated by ultracentrifugation as previously described (65, 66).

Insulin Signaling and Western Blotting. IRS-1– and IRS-2–associated PI3K activity were determined as previously described (38). Briefly, IRS-1– and

IRS-2–associated PI3K activities were measured in liver and muscle extracts after immunoprecipitation with IRS-1 antibody (BD Transduction Laboratories) or IRS-2 antibody (Cell Signaling)/agarose conjugate overnight at 4 °C. Then, the incorporation of ^{32}P into PI to yield phosphatidylinositol-3-monophosphate was measured to determine the IRS-1– and IRS-2–associated PI3K activity.

Proteins from tissue lysate were separated by 4–12% sodium dodecyl sulfate polyacrylamide gel electrophoresis (SDS/PAGE) (Invitrogen) and then transferred onto polyvinylidene difluoride membranes (Millipore). After blocking in 5% bovine serum albumin (BSA)/Tris-buffered saline with Tween (TBST) (10 mM Tris, 100 mM NaCl, and 0.1% Tween-20) solution, membranes were incubated overnight at 4 °C with antibodies obtained from Cell Signaling Technology (pIRK-Y1162, IRK, GAPDH, pAkt-S473, Akt, pJNK, peNOS, AMPK, pAMPK, ACC, pACC, Perilipin, ATGL, pHSL, and HSL), BD Transduction Laboratories (PKCε, PKCθ, and eNOS), Shulman Lab (pIRK T1160) (40), EMD Millipore (JNK), VALAsciences (pPerilipin), and Abcam (Na/K ATPase and pATGL). After washing with TBST, membranes were incubated with horseradish peroxidase-conjugated secondary antibodies and detection was performed with enhanced chemiluminescence. For assaying the IRK-T1160 phosphorylation, after protein concentration quantitation, protein samples were first immunoprecipitated by Dynabeads M-270 Epoxy (Invitrogen) conjugated with D2 anti-IR alpha-subunit antibody. The primary antibody solution was diluted 1:100–1:200 for pIRK-T1160 detection.

Hepatic VLDL-TG Production. Hepatic VLDL-TG production was assessed as previously described (67). In order to determine the basal plasma TAG level, after overnight fasting, blood samples were collected. Mice were injected intraperitoneally with poloxamer 407 (1 g/kg of body weight; Sigma Aldrich) to inhibit tissue LPL activity, and blood samples were collected at 1, 2, 3, and 4 h after injection. The VLDL-TG production rate was calculated by the resultant increase in plasma TAG concentrations.

Oral Lipid Tolerance Test and Tissue-Specific Lipid Uptake. Lipid clearance and tissue-specific uptake were measured by using [9,10-^{3}H] triolein as previously described (67, 68). After overnight fasting, mice received a gavage of a mixed meal: 10 μL/g 10% dextrose in Intralipid (20%; Abbott Laboratories) conjugated with 10 μCi of [9,10-^{3}H]triolein (PerkinElmer). Blood was collected by tail

vein massage at 0, 1, 2, 3, and 4 h for plasma TAG determination. Plasma TAG concentrations was measured by a standard kit (Sekisui/Fujifilm), and ^{3}H radioactivity was measured by scintillation counter.

Lipoprotein Lipase Activity Assay. LPL activity was assessed as previously described (69, 70). Briefly, for plasma LPL activity, blood samples were collected after overnight fasting to determine basal plasma TAG and LPL activity. Then, mice were injected i.v. with heparin (50 U/kg of body weight) and blood samples were taken after 10-min injection. Postheparin plasma LPL activity was assessed by a fluorometric assay (Cell Biolabs). Tissue LPL was extracted by incubation of tissue at 37 °C for 1 h in phosphate-buffered saline (PBS) with 5 U/mL heparin and 2 mg/mL BSA. Samples were centrifuged at $900 \times g$ for 15 min, and the supernatant tissue LPL activities were measured in the presence of heat-inactivated mouse serum using a fluorometric assay (Cell Biolabs).

Statistical Analysis. All data are expressed as the mean ± SEM. Results were assessed using two-tailed unpaired Student's t test or two-way ANOVA. $*P < 0.05$, $**P < 0.01$, $*P < 0.05$, $**P < 0.01$, $***P < 0.001$, $****P < 0.0001$. GraphPad Prism 8.0 was used for all statistical analyses. In most cases, $n = 6–9$ per group, unless otherwise indicated in the figure legends.

1. V. Bermudez *et al.*, Prevalence and associated factors of insulin resistance in adults from Maracaibo city, Venezuela. *Adv. Prev. Med.* **2016**, 9405105 (2016).
2. Y. Zheng, S. H. Ley, F. B. Hu, Global aetiology and epidemiology of type 2 diabetes mellitus and its complications. *Nat. Rev. Endocrinol.* **14**, 88–98 (2018).
3. G. I. Shulman, Ectopic fat in insulin resistance, dyslipidemia, and cardiometabolic disease. *N. Engl. J. Med.* **371**, 1131–1141 (2014).
4. V. T. Samuel, G. I. Shulman, The pathogenesis of insulin resistance: Integrating signaling pathways and substrate flux. *J. Clin. Invest.* **126**, 12–22 (2016).
5. V. T. Samuel, G. I. Shulman, Mechanisms for insulin resistance: Common threads and missing links. *Cell* **148**, 852–871 (2012).
6. M. Laakso, J. Kuusisto, Insulin resistance and hyperglycaemia in cardiovascular disease development. *Nat. Rev. Endocrinol.* **10**, 293–302 (2014).
7. M. Iwabu *et al.*, Adiponectin and AdipoR1 regulate PGC-1alpha and mitochondria by Ca(2+) and AMPK/SIRT1. *Nature* **464**, 1313–1319 (2010).
8. N. Maeda *et al.*, Diet-induced insulin resistance in mice lacking adiponectin/ACRP30. *Nat. Med.* **8**, 731–737 (2002).
9. K. Hotta *et al.*, Plasma concentrations of a novel, adipose-specific protein, adiponectin, in type 2 diabetic patients. *Arterioscler. Thromb. Vasc. Biol.* **20**, 1595–1599 (2000).
10. C. M. Halleux *et al.*, Secretion of adiponectin and regulation of apM1 gene expression in human visceral adipose tissue. *Biochem. Biophys. Res. Commun.* **288**, 1102–1107 (2001).
11. J. Fruebis *et al.*, Proteolytic cleavage product of 30-kDa adipocyte complement-related protein increases fatty acid oxidation in muscle and causes weight loss in mice. *Proc. Natl. Acad. Sci. U.S.A.* **98**, 2005–2010 (2001).
12. E. Tomas *et al.*, Enhanced muscle fat oxidation and glucose transport by ACRP30 globular domain: Acetyl-CoA carboxylase inhibition and AMP-activated protein kinase activation. *Proc. Natl. Acad. Sci. U.S.A.* **99**, 16309–16313 (2002).
13. H. N. Jones, T. Jansson, T. L. Powell, Full-length adiponectin attenuates insulin signaling and inhibits insulin-stimulated amino Acid transport in human primary trophoblast cells. *Diabetes* **59**, 1161–1170 (2010).
14. T. Yamauchi *et al.*, Adiponectin stimulates glucose utilization and fatty-acid oxidation by activating AMP-activated protein kinase. *Nat. Med.* **8**, 1288–1295 (2002).
15. A. H. Berg, T. P. Combs, X. Du, M. Brownlee, P. E. Scherer, The adipocyte-secreted protein Acrp30 enhances hepatic insulin action. *Nat. Med.* **7**, 947–953 (2001).
16. R. A. Miller *et al.*, Adiponectin suppresses gluconeogenic gene expression in mouse hepatocytes independent of LKB1-AMPK signaling. *J. Clin. Invest.* **121**, 2518–2528 (2011).
17. A. Xu *et al.*, The fat-derived hormone adiponectin alleviates alcoholic and nonalcoholic fatty liver diseases in mice. *J. Clin. Invest.* **112**, 91–100 (2003).
18. W. L. Holland *et al.*, Receptor-mediated activation of ceramidase activity initiates the pleiotropic actions of adiponectin. *Nat. Med.* **17**, 55–63 (2011).
19. P. J. Randle, P. B. Garland, C. N. Hales, E. A. Newsholme, The glucose fatty-acid cycle. Its role in insulin sensitivity and the metabolic disturbances of diabetes mellitus. *Lancet* **1**, 785–789 (1963).
20. G. W. Cline *et al.*, Impaired glucose transport as a cause of decreased insulin-stimulated muscle glycogen synthesis in type 2 diabetes. *N. Engl. J. Med.* **341**, 240–246 (1999).
21. A. Dresner *et al.*, Effects of free fatty acids on glucose transport and IRS-1-associated phosphatidylinositol 3-kinase activity. *J. Clin. Invest.* **103**, 253–259 (1999).
22. M. Pagadala, T. Kasumov, A. J. McCullough, N. N. Zein, J. P. Kirwan, Role of ceramides in nonalcoholic fatty liver disease. *Trends Endocrinol. Metab.* **23**, 365–371 (2012).
23. S. Stratford, K. L. Hoehn, F. Liu, S. A. Summers, Regulation of insulin action by ceramide: Dual mechanisms linking ceramide accumulation to the inhibition of Akt/protein kinase B. *J. Biol. Chem.* **279**, 36608–36615 (2004).
24. A. U. Blachnio-Zabielska, M. Chacinska, M. H. Vendelbo, P. Zabielski, The crucial role of C18-Cer in fat-induced skeletal muscle insulin resistance. *Cell. Physiol. Biochem.* **40**, 1207–1220 (2016).
25. M. C. Petersen *et al.*, Insulin receptor Thr1160 phosphorylation mediates lipid-induced hepatic insulin resistance. *J. Clin. Invest.* **126**, 4361–4371 (2016).
26. V. T. Samuel *et al.*, Inhibition of protein kinase Cepsilon prevents hepatic insulin resistance in nonalcoholic fatty liver disease. *J. Clin. Invest.* **117**, 739–745 (2007).
27. M. C. Petersen, G. I. Shulman, Roles of diacylglycerols and ceramides in hepatic insulin resistance. *Trends Pharmacol. Sci.* **38**, 649–665 (2017).
28. J. Szendroedi *et al.*, Role of diacylglycerol activation of PKCθ in lipid-induced muscle insulin resistance in humans. *Proc. Natl. Acad. Sci. U.S.A.* **111**, 9597–9602 (2014).
29. J. D. Song *et al.*, Dissociation of muscle insulin resistance from alterations in mitochondrial substrate preference. *Cell Metab.* **32**, 726–735.e5 (2020).
30. C. Yu *et al.*, Mechanism by which fatty acids inhibit insulin activation of insulin receptor substrate-1 (IRS-1)-associated phosphatidylinositol 3-kinase activity in muscle. *J. Biol. Chem.* **277**, 50230–50236 (2002).
31. M. Roden *et al.*, Mechanism of free fatty acid-induced insulin resistance in humans. *J. Clin. Invest.* **97**, 2859–2865 (1996).
32. A. Guilherme, F. Henriques, A. H. Bedard, M. P. Czech, Molecular pathways linking adipose innervation to insulin action in obesity and diabetes mellitus. *Nat. Rev. Endocrinol.* **15**, 207–225 (2019).
33. P. Morigny, M. Houssier, E. Mouisel, D. Langin, Adipocyte lipolysis and insulin resistance. *Biochimie* **125**, 259–266 (2016).
34. J. Y. Kim *et al.*, Obesity-associated improvements in metabolic profile through expansion of adipose tissue. *J. Clin. Invest.* **117**, 2621–2637 (2007).
35. Y. Fu, N. Luo, R. L. Klein, W. T. Garvey, Adiponectin promotes adipocyte differentiation, insulin sensitivity, and lipid accumulation. *J. Lipid Res.* **46**, 1369–1379 (2005).
36. G. S. Hotamisligil, Inflammation and metabolic disorders. *Nature* **444**, 860–867 (2006).

37. M. E. Griffin et al., Free fatty acid-induced insulin resistance is associated with activation of protein kinase C theta and alterations in the insulin signaling cascade. *Diabetes* **48**, 1270–1274 (1999).

38. J. K. Kim et al., PKC-theta knockout mice are protected from fat-induced insulin resistance. *J. Clin. Invest.* **114**, 823–827 (2004).

39. L. T. Boni, R. R. Rando, The nature of protein kinase C activation by physically defined phospholipid vesicles and diacylglycerols. *J. Biol. Chem.* **260**, 10819–10825 (1985).

40. K. Lyu et al., A membrane-bound diacylglycerol species induces PKCE-Mediated hepatic insulin resistance. *Cell Metab.* **32**, 654–664.e5 (2020).

41. H. Nomura et al., Stereospecificity of diacylglycerol for stimulus-response coupling in platelets. *Biochem. Biophys. Res. Commun.* **140**, 1143–1151 (1986).

42. T. Hla, R. Kolesnick, C16:0-ceramide signals insulin resistance. *Cell Metab.* **20**, 703–705 (2014).

43. E. Sokolowska, A. Blachnio-Zabielska, The role of ceramides in insulin resistance. *Front. Endocrinol. (Lausanne)* **10**, 577 (2019).

44. H. Bays, L. Mandarino, R. A. DeFronzo, Role of the adipocyte, free fatty acids, and ectopic fat in pathogenesis of type 2 diabetes mellitus: Peroxisomal proliferator-activated receptor agonists provide a rational therapeutic approach. *J. Clin. Endocrinol. Metab.* **89**, 463–478 (2004).

45. R. J. Perry et al., Non-invasive assessment of hepatic mitochondrial metabolism by positional isotopomer NMR tracer analysis (PINTA). *Nat. Commun.* **8**, 798 (2017).

46. V. A. Lira et al., Nitric oxide and AMPK cooperatively regulate PGC-1 in skeletal muscle cells. *J. Physiol.* **588**, 3551–3566 (2010).

47. P. H. Weinstock et al., Lipoprotein lipase controls fatty acid entry into adipose tissue, but fat mass is preserved by endogenous synthesis in mice deficient in adipose tissue lipoprotein lipase. *Proc. Natl. Acad. Sci. U.S.A.* **94**, 10261–10266 (1997).

48. T. Yamauchi et al., The fat-derived hormone adiponectin reverses insulin resistance associated with both lipoatrophy and obesity. *Nat. Med.* **7**, 941–946 (2001).

49. A. E. Achari, S. K. Jain, Adiponectin, a therapeutic target for obesity, diabetes, and endothelial dysfunction. *Int. J. Mol. Sci.* **18**, 1321 (2017).

50. R. S. Ahima, J. S. Flier, Adipose tissue as an endocrine organ. *Trends Endocrinol. Metab.* **11**, 327–332 (2000).

51. V. Mohamed-Ali, J. H. Pinkney, S. W. Coppack, Adipose tissue as an endocrine and paracrine organ. *Int. J. Obes. Relat. Metab. Disord.* **22**, 1145–1158 (1998).

52. R. J. Perry et al., Leptin mediates postprandial increases in body temperature through hypothalamus-adrenal medulla-adipose tissue crosstalk. *J. Clin. Invest.* **130**, 2001–2016 (2020).

53. R. J. Perry et al., Leptin mediates a glucose-fatty acid cycle to maintain glucose homeostasis in starvation. *Cell* **172**, 234–248.e17 (2018).

54. M. Awazawa et al., Adiponectin enhances insulin sensitivity by increasing hepatic IRS-2 expression via a macrophage-derived IL-6-dependent pathway. *Cell Metab.* **13**, 401–412 (2011).

55. M. Awazawa et al., Adiponectin suppresses hepatic SREBP1c expression in an AdipoR1/LKB1/AMPK dependent pathway. *Biochem. Biophys. Res. Commun.* **382**, 51–56 (2009).

56. K. Hotta et al., Circulating concentrations of the adipocyte protein adiponectin are decreased in parallel with reduced insulin sensitivity during the progression to type 2 diabetes in rhesus monkeys. *Diabetes* **50**, 1126–1133 (2001).

57. C. Weyer et al., Hypoadiponectinemia in obesity and type 2 diabetes: Close association with insulin resistance and hyperinsulinemia. *J. Clin. Endocrinol. Metab.* **86**, 1930–1935 (2001).

58. T. P. Combs et al., A transgenic mouse with a deletion in the collagenous domain of adiponectin displays elevated circulating adiponectin and improved insulin sensitivity. *Endocrinology* **145**, 367–383 (2004).

59. N. Kubota et al., Disruption of adiponectin causes insulin resistance and neointimal formation. *J. Biol. Chem.* **277**, 25863–25866 (2002).

60. R. J. Perry et al., Hepatic acetyl CoA links adipose tissue inflammation to hepatic insulin resistance and type 2 diabetes. *Cell* **160**, 745–758 (2015).

61. R. J. Perry et al., Leptin mediates a glucose-fatty acid cycle to maintain glucose homeostasis in starvation. *Cell* **172**, 234–248.e17 (2018).

62. G. S. Cuendet, E. G. Loten, B. Jeanrenaud, A. E. Renold, Decreased basal, noninsulin-stimulated glucose uptake and metabolism by skeletal soleus muscle isolated from obese-hyperglycemic (ob/ob) mice. *J. Clin. Invest.* **58**, 1078–1088 (1976).

63. A. Abulizi et al., Membrane bound diacylglycerols explain the dissociation of hepatic insulin resistance from steatosis in MTTP$^{-/-}$ mice. *J. Lipid Res.*, 10.1194/jlr.RA119000586 (2020).

64. E. G. Bligh, W. J. Dyer, A rapid method of total lipid extraction and purification. *Can. J. Biochem. Physiol.* **37**, 911–917 (1959).

65. N. Kumashiro et al., Cellular mechanism of insulin resistance in nonalcoholic fatty liver disease. *Proc. Natl. Acad. Sci. U.S.A.* **108**, 16381–16385 (2011).

66. V. T. Samuel et al., Mechanism of hepatic insulin resistance in non-alcoholic fatty liver disease. *J. Biol. Chem.* **279**, 32345–32353 (2004).

67. J. P. Camporez et al., ApoA5 knockdown improves whole-body insulin sensitivity in high-fat-fed mice by reducing ectopic lipid content. *J. Lipid Res.* **56**, 526–536 (2015).

68. H. Y. Lee et al., Apolipoprotein CIII overexpressing mice are predisposed to diet-induced hepatic steatosis and hepatic insulin resistance. *Hepatology* **54**, 1650–1660 (2011).

69. D. F. Vatner et al., Angptl8 antisense oligonucleotide improves adipose lipid metabolism and prevents diet-induced NAFLD and hepatic insulin resistance in rodents. *Diabetologia* **61**, 1435–1446 (2018).

70. H. Yagyu et al., Lipoprotein lipase (LpL) on the surface of cardiomyocytes increases lipid uptake and produces a cardiomyopathy. *J. Clin. Invest.* **111**, 419–426 (2003).

MEDICAL SCIENCES